Global patterns of urban heat shaped by climate and morphology

Siwoo Lee[1, †], Cheolhee Yoo[2, 3, †], Bokyung Son[1], Dongjin Cho[4], Jungho Im[1, 5, 6, *], and TC Chakraborty[7]

[1] Department of Civil, Urban, Earth, and Environmental Engineering, Ulsan National Institute of Science and Technology (UNIST), Ulsan, South Korea

[2] Smart City Convergence Major, Pusan National University, Busan, South Korea

[3] Department of Urban Planning and Engineering, Pusan National University, Busan, South Korea

[4] Environmental Planning Institute, Seoul National University, Seoul, South Korea

[5] Graduate School of Artificial Intelligence, UNIST, Ulsan, South Korea

[6] Graduate School of Carbon Neutrality, UNIST, Ulsan, South Korea

[7] Pacific Northwest National Laboratory, Richland, WA, USA

* Corresponding author: Jungho Im (ersgis@unist.ac.kr)

† These authors contributed equally: Siwoo Lee, Cheolhee Yoo

Supplementary Information

- Supplementary Fig. 1–17
- Supplementary Table 1–2
- Supplementary References

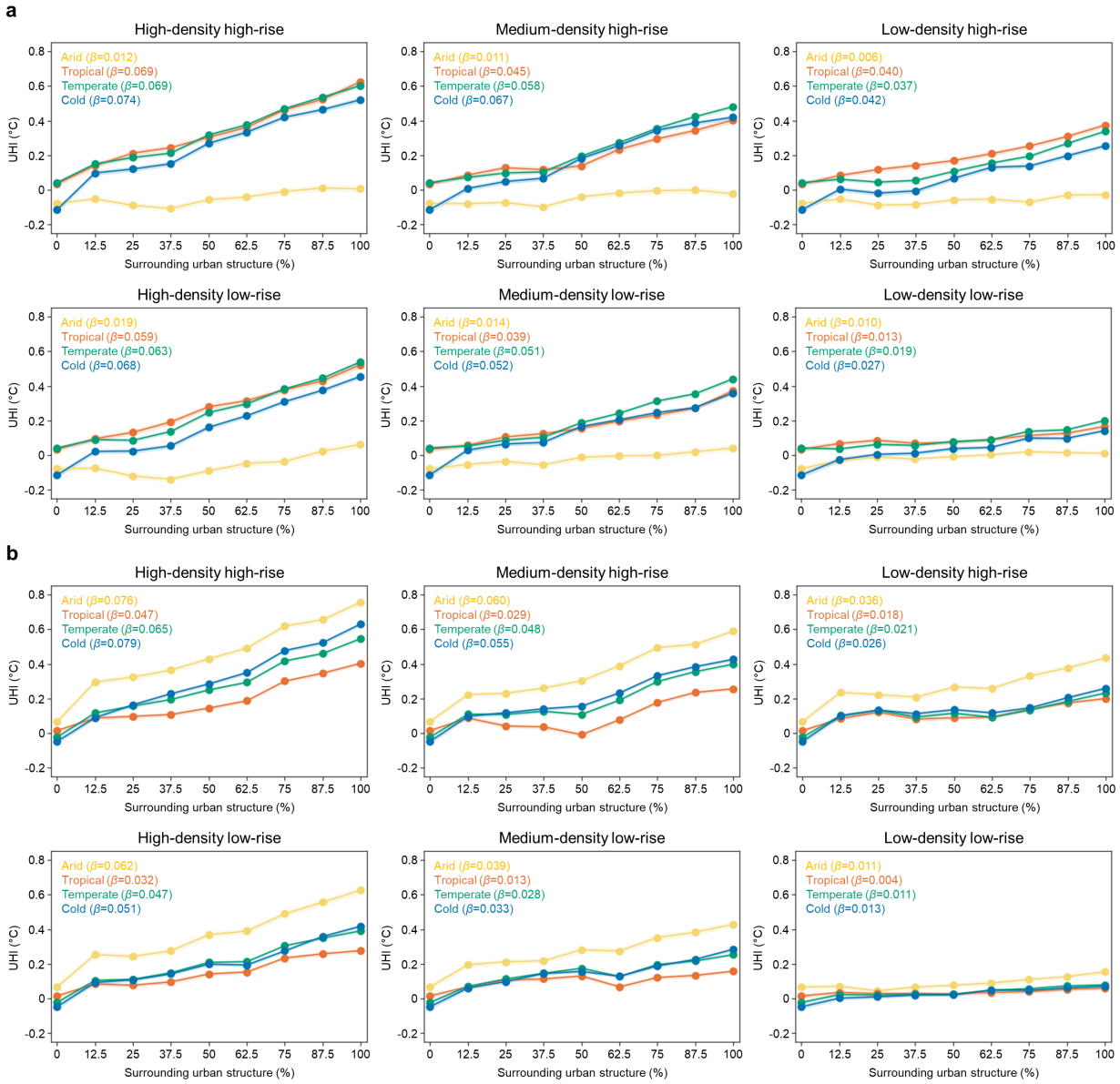

Supplementary Fig. 1 | Thermal response to progressive increases in surrounding urban structure. Predicted urban heat island (UHI) intensity as the eight surrounding pixels are progressively converted from rural to urban morphology, corresponding to 0–100% surrounding urban structure. Results are shown for each central urban morphology class across four climate zones under daytime (**a**) and nighttime (**b**) conditions. Regression slopes (β) indicate the fitted change in UHI associated with each additional surrounding pixel converted from non-built-up to built-up types. Shaded areas denote the 95% confidence interval based on variation among central urban morphology classes.

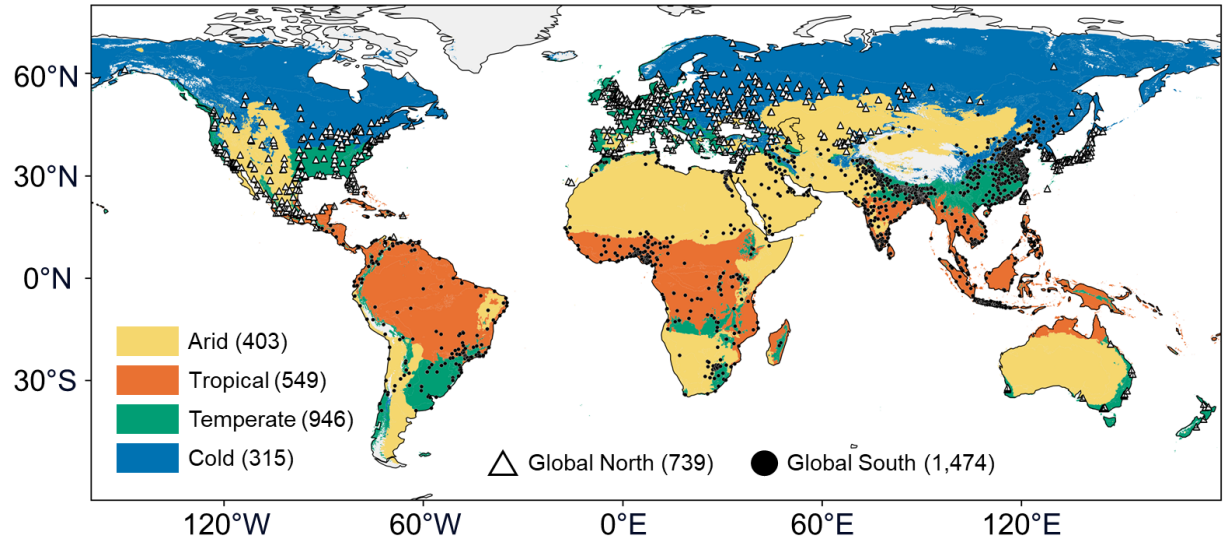

Supplementary Fig. 2 | Spatial distribution of selected cities across climate zones. Geographic distribution of the 2,213 selected urban areas used in this study. Each dot represents the centroid of a city with an urban boundary larger than 50 km², derived from the Global Human Settlement Urban Centre Database[1] in 2020. City centroids are marked by symbols: cities in *the* Global South are shown as black circles (1,474 cities), while cities in the Global North are shown as white triangles with black borders (739 cities). The background *shading* indicates dominant Köppen–Geiger climate zones[2]: arid (403 cities), tropical (549 cities), temperate (946 cities), and cold (315 cities). Basemap from Natural Earth (https://www.naturalearthdata.com).

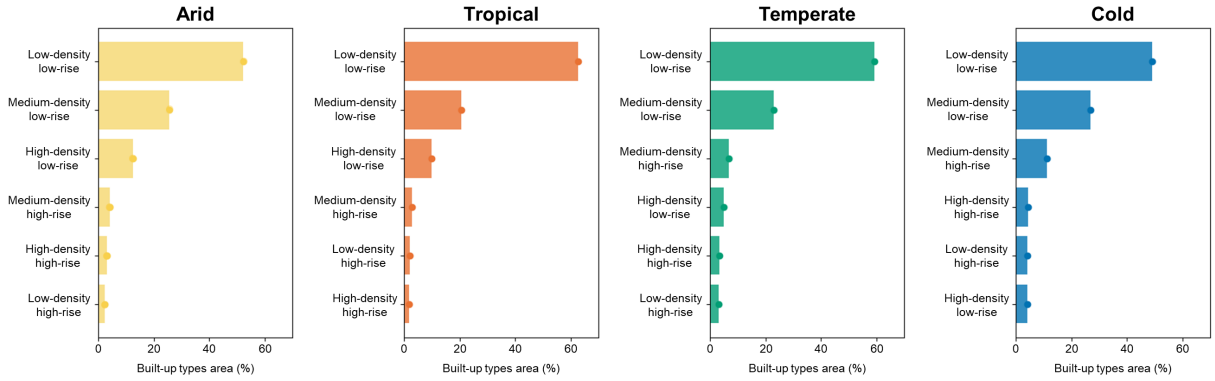

Supplementary Fig. 3 | Composition of built environments categorized by six built-up types across climate zones. Horizontal bars show the average area fraction of the six built-up urban morphology types in cities from the arid (403 cities), tropical (549 cities), temperate (946 cities), and cold (315 cities) climate zones. Morphology types are classified by building density and height, and percentages are expressed relative to the total built-up area. Classes are ordered by abundance within each climate zone, and circular markers indicate the corresponding mean values.

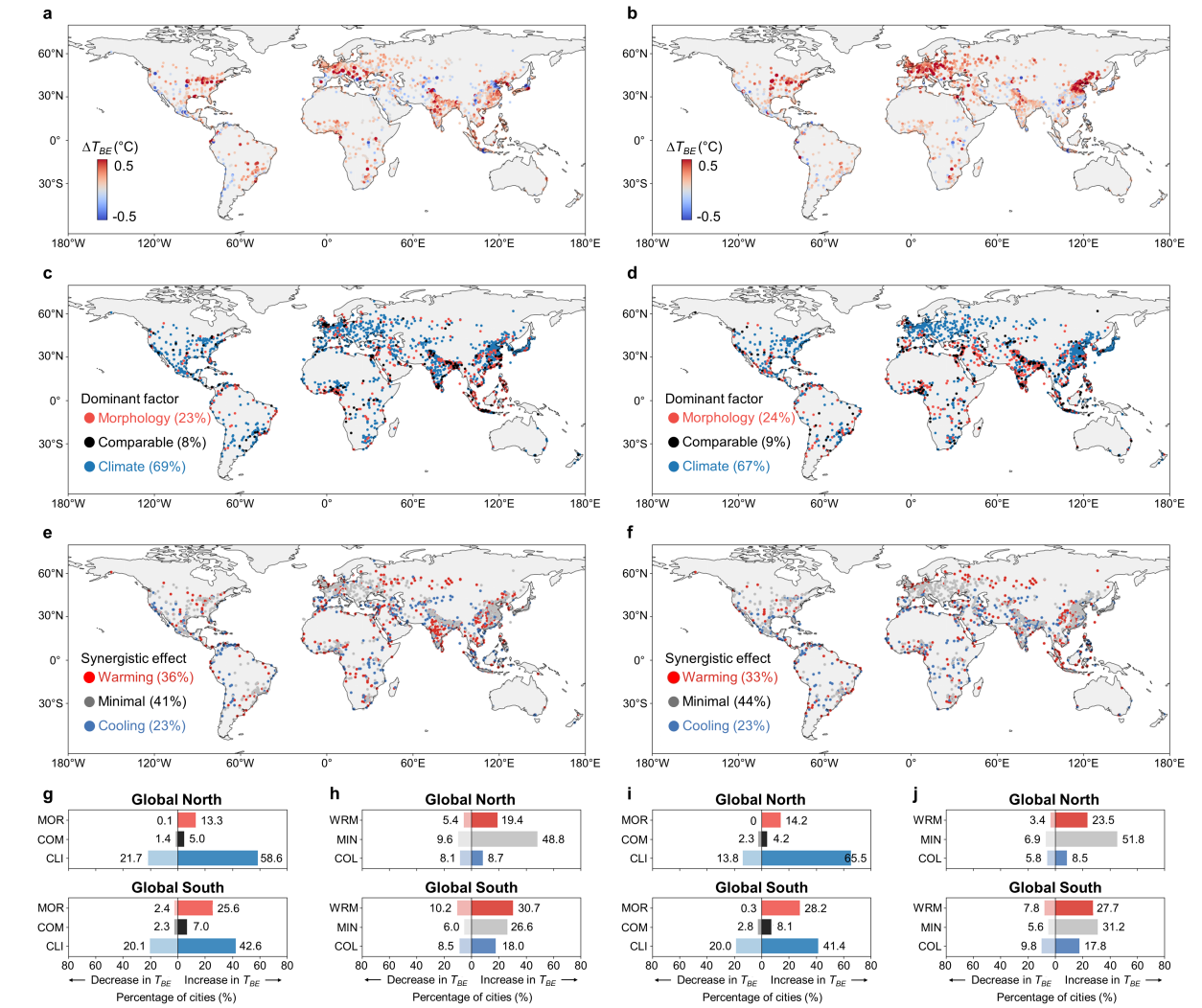

Supplementary Fig. 4 | Global distribution of projected changes in the thermal impact of the surrounding built environment (T_{BE}) and their attribution to climate, morphology, and interaction under SSP1. a, b Spatial distribution of projected differences in T_{BE} (ΔT_{BE}) between present-day (2020) and future (2050) conditions for daytime (**a**) and nighttime (**b**). Positive values indicate intensification of T_{BE}, whereas negative values indicate weakening. **c, d** Spatial distribution of the dominant driver of projected T_{BE} change for daytime (**c**) and nighttime (**d**): morphology (MOR), comparable (COM), or climate (CLI). Numbers indicate the proportion of all 2,213 cities assigned to each category. Dominance was quantified using a normalized score based on the relative absolute magnitudes of the climate-only and morphology-only contributions. The climate-only contribution was calculated by applying future long-term climate conditions while holding urban morphology constant at its present state, whereas the morphology-only contribution was calculated by applying future urban morphological conditions while holding climate constant. Cities are classified as climate when the score is > 0.1, morphology when it is < −0.1, and comparable when it falls within ±0.1 of zero. **e, f** Synergistic effects between climate change and urban morphological change on projected daytime (**e**) and nighttime (**f**) TBE change, calculated as the residual between projected T_{BE} under future conditions and the sum of the climate-only and morphology-only changes. Numbers indicate the percentage of all 2,213 cities assigned to each synergistic class. Synergistic effects are defined using the same threshold: warming (WRM) for values > 0.1, cooling (COL) for values < −0.1, and minimal (MIN) interaction

for values within ±0.1. **g, h** Percentage of cities in each dominant-driver category (**g**) and synergistic-effect category (**h**) for the Global North and Global South under daytime conditions. Leftward bars from zero (lighter shading) indicate cities with decreasing T_{BE} and rightward bars from zero (darker shading) indicate cities with increasing T_{BE}. **i, j** Same as **g** and **h**, but for nighttime conditions. Basemap from Natural Earth (https://www.naturalearthdata.com).

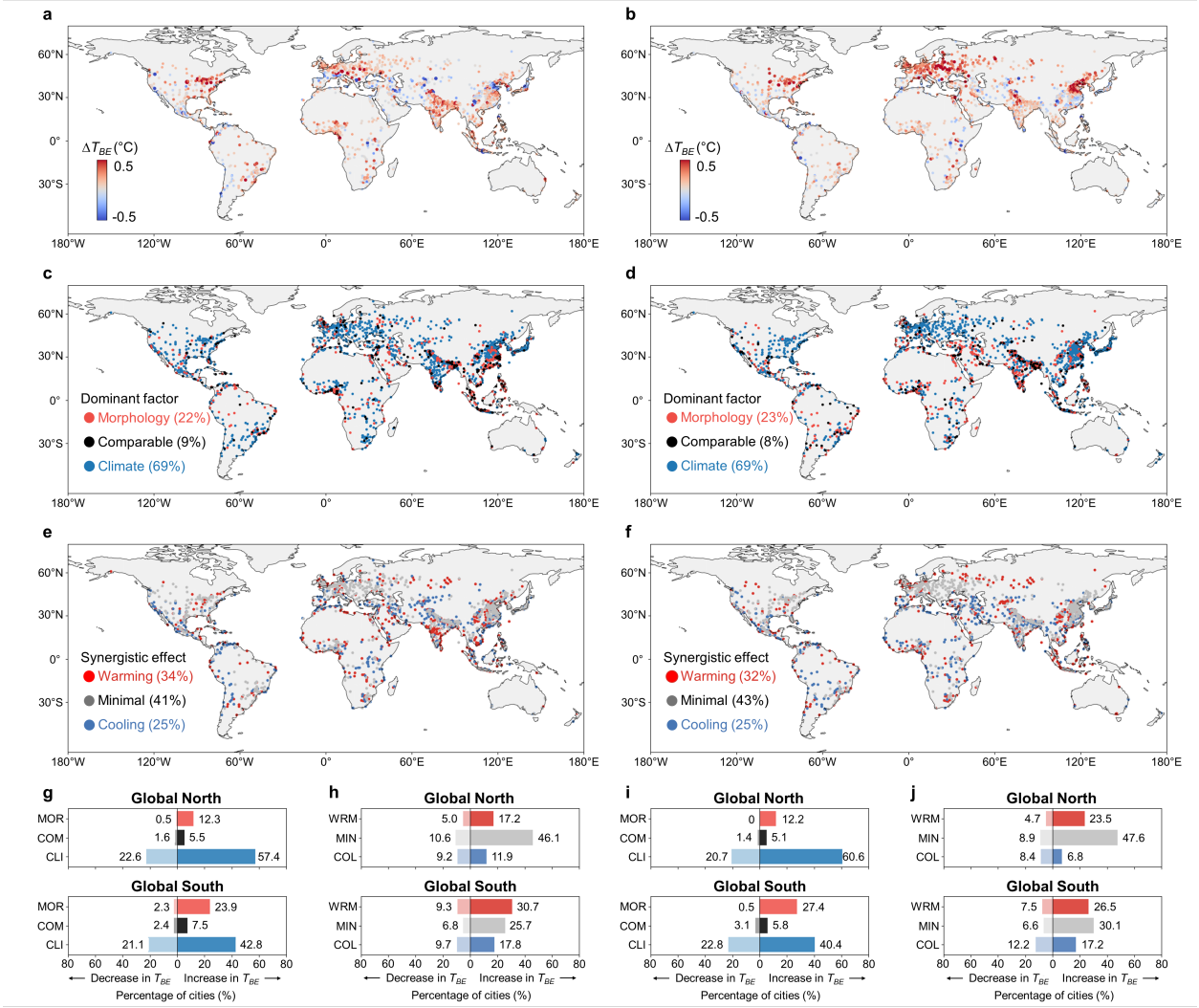

Supplementary Fig. 5 | Same as Supplementary Fig. 4 but under SSP2.

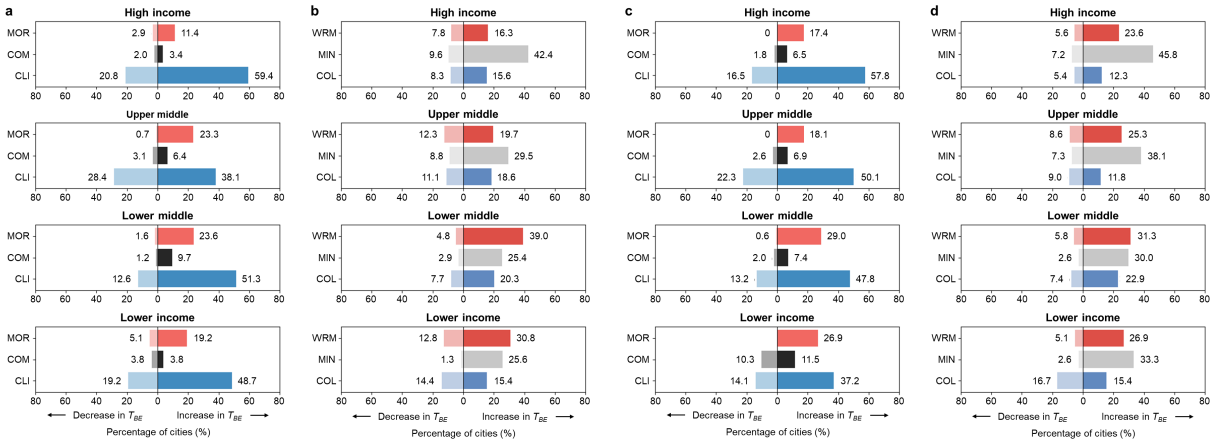

Supplementary Fig. 6 | Income level differences in dominant factors and synergistic effect of projected thermal impact of the surrounding built environment (T_{BE}) change under SSP5. a, c, Percentage of cities in each dominant-driver category for projected daytime (**a**) and nighttime (**c**) T_{BE} change, stratified by income level (high income, upper middle income, lower middle income, and low income), using the Global Human Settlement Urban Centre Database[1]. Cities are classified as Morphology (MOR), Comparable (COM), or Climate (CLI), based on the normalized dominance score comparing the relative absolute magnitudes of the climate-only and morphology-only contributions. **b, d,** Percentage of cities in each synergistic effect category for projected daytime (**b**) and nighttime (**d**) T_{BE} change, stratified by income level. Synergistic effects are classified as Warming (WRM), Minimal (MIN), or Cooling (COL), using the same ±0.1 threshold applied in **Fig. 4**. Leftward bars from zero (lighter shading) indicate cities with decreasing T_{BE} and rightward bars from zero (darker shading) indicate cities with increasing T_{BE}. Numbers denote the percentage of cities within each income group.

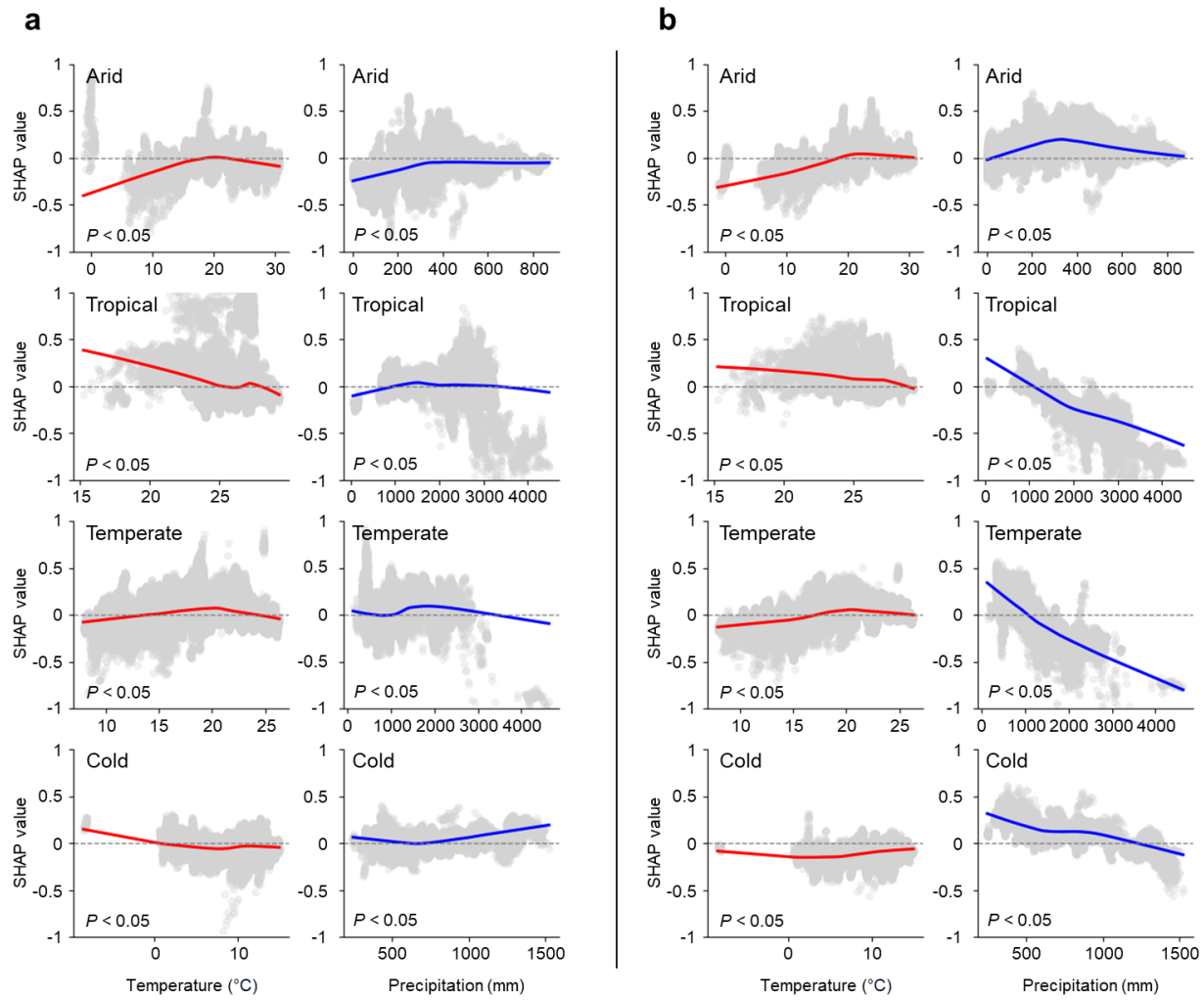

Supplementary Fig. 7 | Climate-specific SHAP contribution patterns of temperature and precipitation on canopy urban heat island. a, SHAP (SHapley Additive exPlanations) dependence plots showing the marginal contributions of long-term mean annual temperature and precipitation to canopy urban heat island intensity across four climate zones. **b**, Same as **a** but for nighttime. Each panel presents SHAP values (y-axis) as a function of the corresponding climatic variable (x-axis), with locally weighted scatterplot smoothing curves overlaid, red for temperature and blue for precipitation. Gray dots represent individual model samples. *P* values are from F-tests comparing linear models with locally weighted scatterplot smoothing fits.

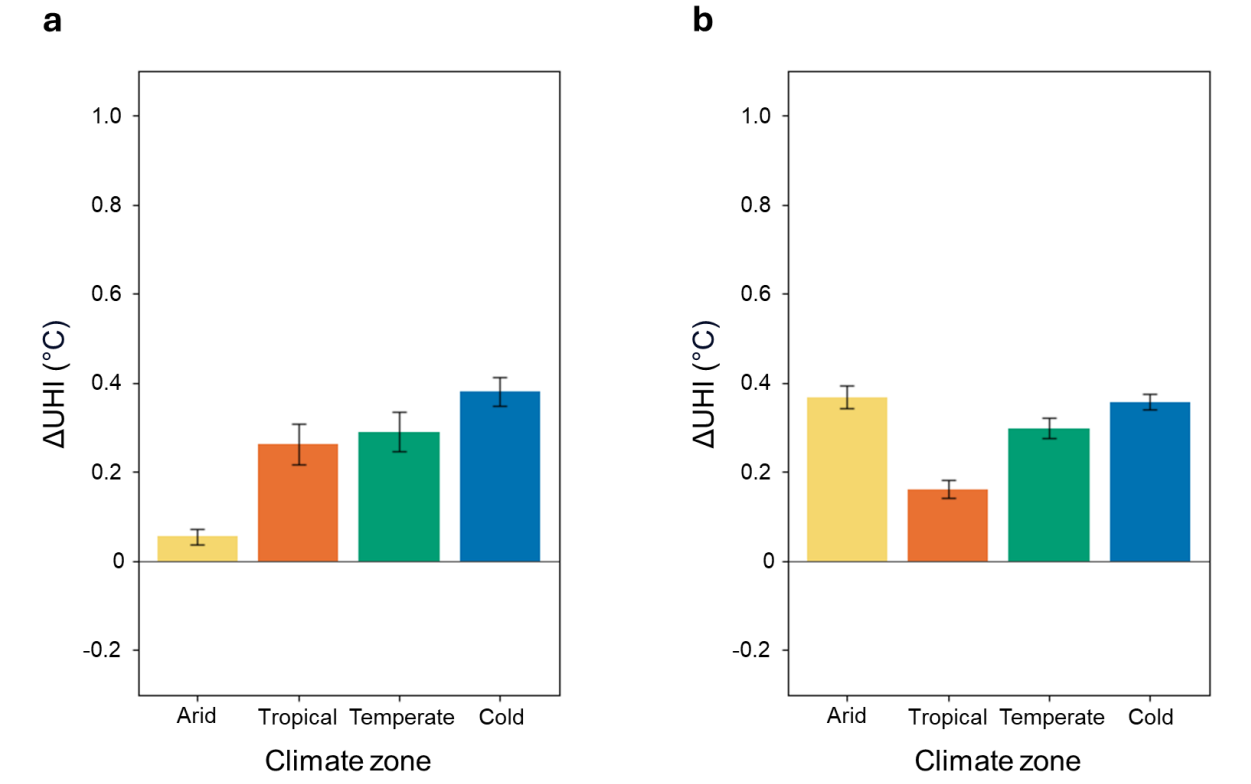

Supplementary Fig. 8 | Random-composition baseline of surrounding thermal impact. Mean predicted changes in surrounding urban morphology-induced UHI change (ΔUHI) for randomly mixed surrounding urban morphology compositions (N = 3,003), relative to the non-built-up surrounded condition, during daytime (**a**) and nighttime (**b**) across arid (403 cities), tropical (549 cities), temperate (946 cities), and cold (315 cities) climate zones. Error bars represent variability across random neighborhood realizations.

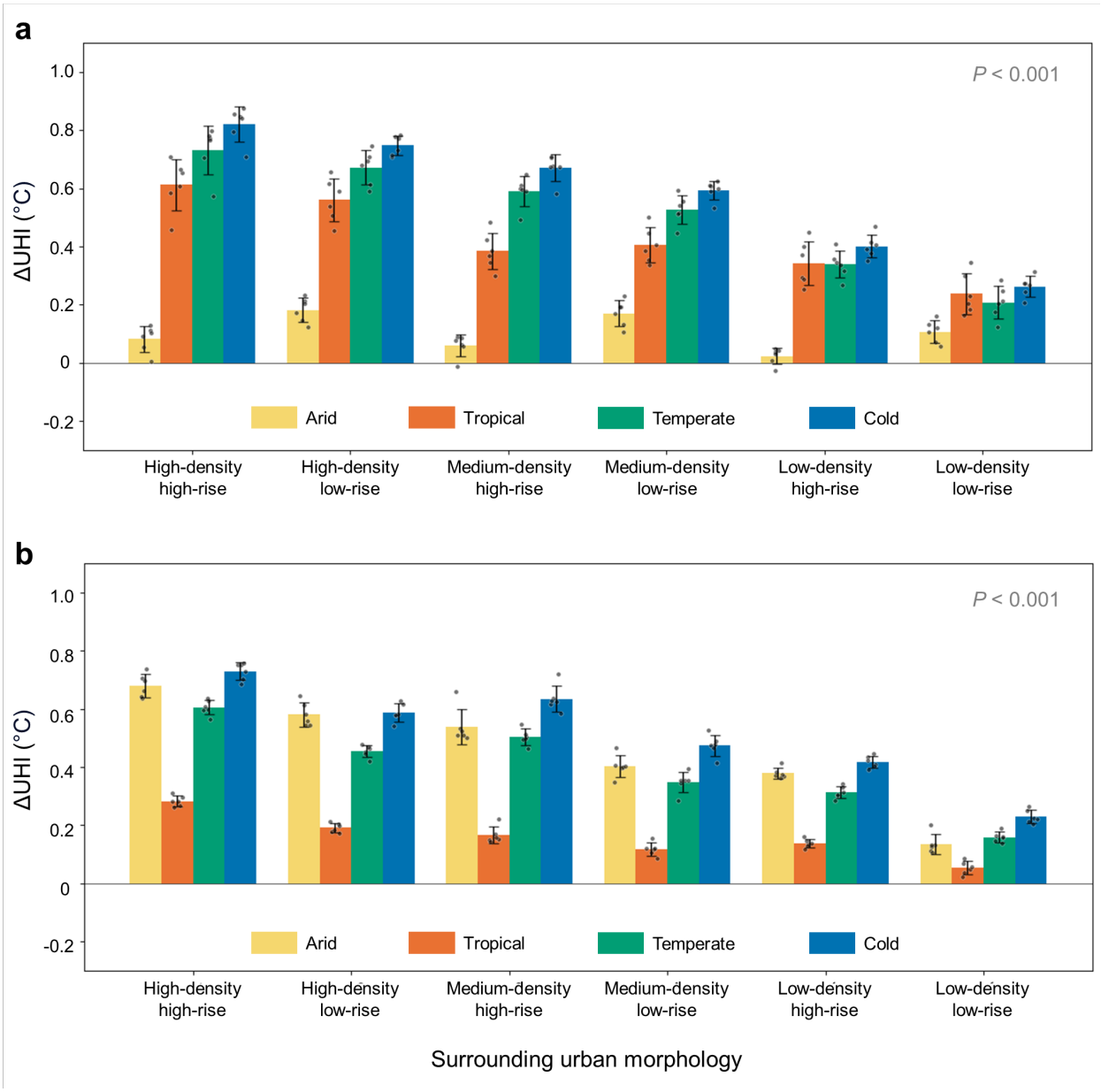

Supplementary Fig. 9 | Surrounding urban morphology-induced urban heat island change (ΔUHI) during summer across climate zones. a, b ΔUHI during the daytime (**a**) and nighttime (**b**), defined as the change in canopy urban heat island (UHI) intensity when adjacent land cover transitions from non-built-up to a given built-up type. Summer is defined as June–August (JJA) in the Northern Hemisphere and December–February (DJF) in the Southern Hemisphere. All six built-up types were applied as central pixels; ΔUHI represents the mean thermal influence of each built-up type, averaged across all combinations of central and surrounding built-up types. Bars indicate the average magnitude of ΔUHI in arid (403 cities), tropical (549 cities), temperate (946 cities), and cold (315 cities) climate zones. Dots indicate the mean ΔUHI values for each central built-up type, and error bars represent the standard deviation across these types. *P* values are from two-way ANOVA.

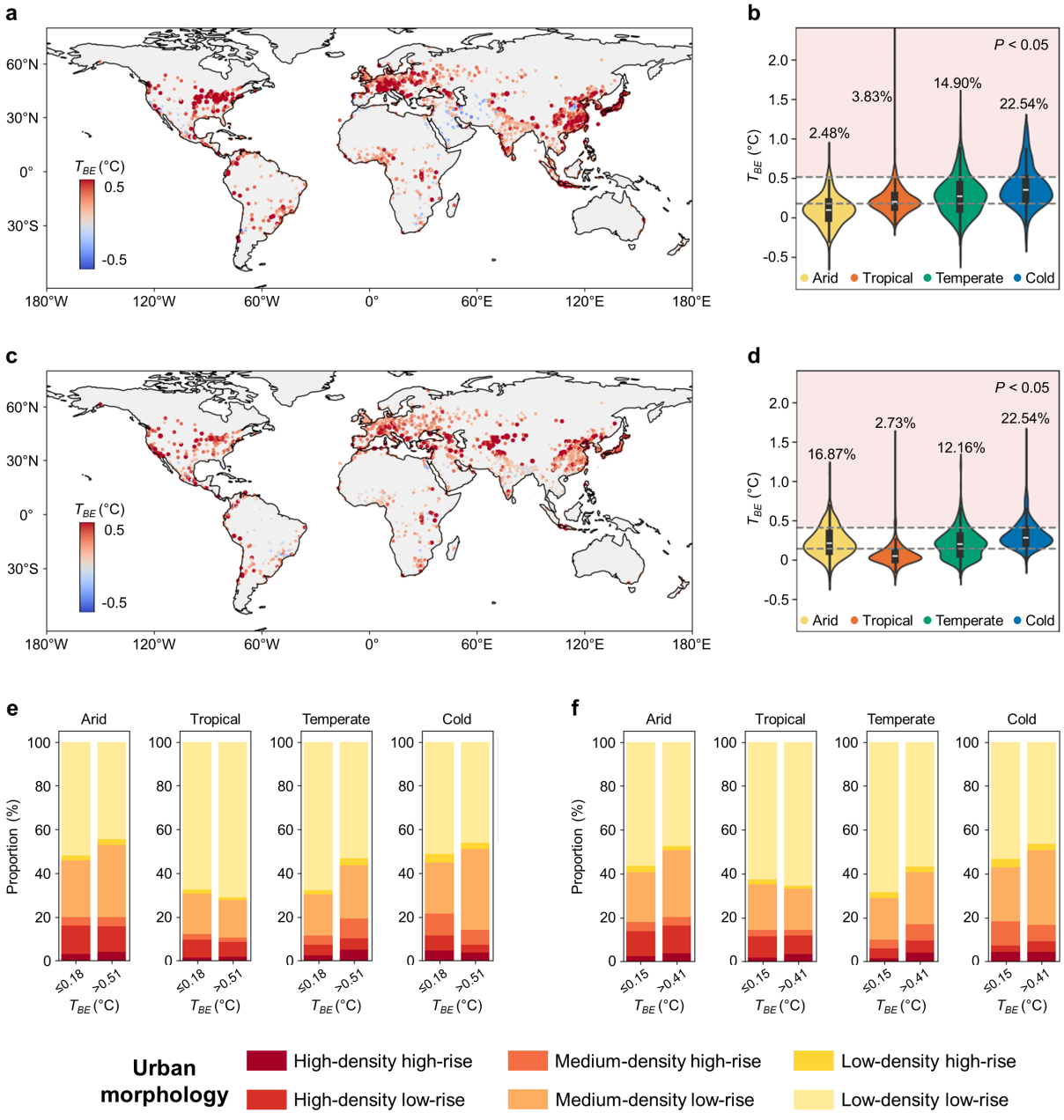

Supplementary Fig. 10 | Spatial and structural distribution of the thermal impact of the surrounding built environment (T_{BE}) during summer. a, c Global distribution of daytime (**a**) and nighttime (**c**) T_{BE} during summer across 2,213 cities, with point color and size indicating T_{BE} magnitude. Summer is defined as June–August (JJA) in the Northern Hemisphere and December–February (DJF) in the Southern Hemisphere. **b, d** Violin plots showing the distributions of daytime (**b**) and nighttime (**d**) T_{BE} by climate zone. Within each violin, the white line indicates the median, the box indicates the interquartile range (IQR), and the whiskers extend to 1.5 × IQR. Horizontal dashed lines indicate category thresholds determined using the Jenks natural breaks method; red-shaded areas correspond to the high-T_{BE} category. Numbers above each violin indicate the proportion of cities classified as high T_{BE} within each climate zone. *P* values are based on the Kruskal–Wallis H test. **e, f** Proportional composition of the six built-up types

for cities grouped by T_{BE} category within each climate zone for daytime (**e**; high: > 0.51 °C; low: ≤ 0.18 °C) and nighttime (**f**). Basemap from Natural Earth (https://www.naturalearthdata.com).

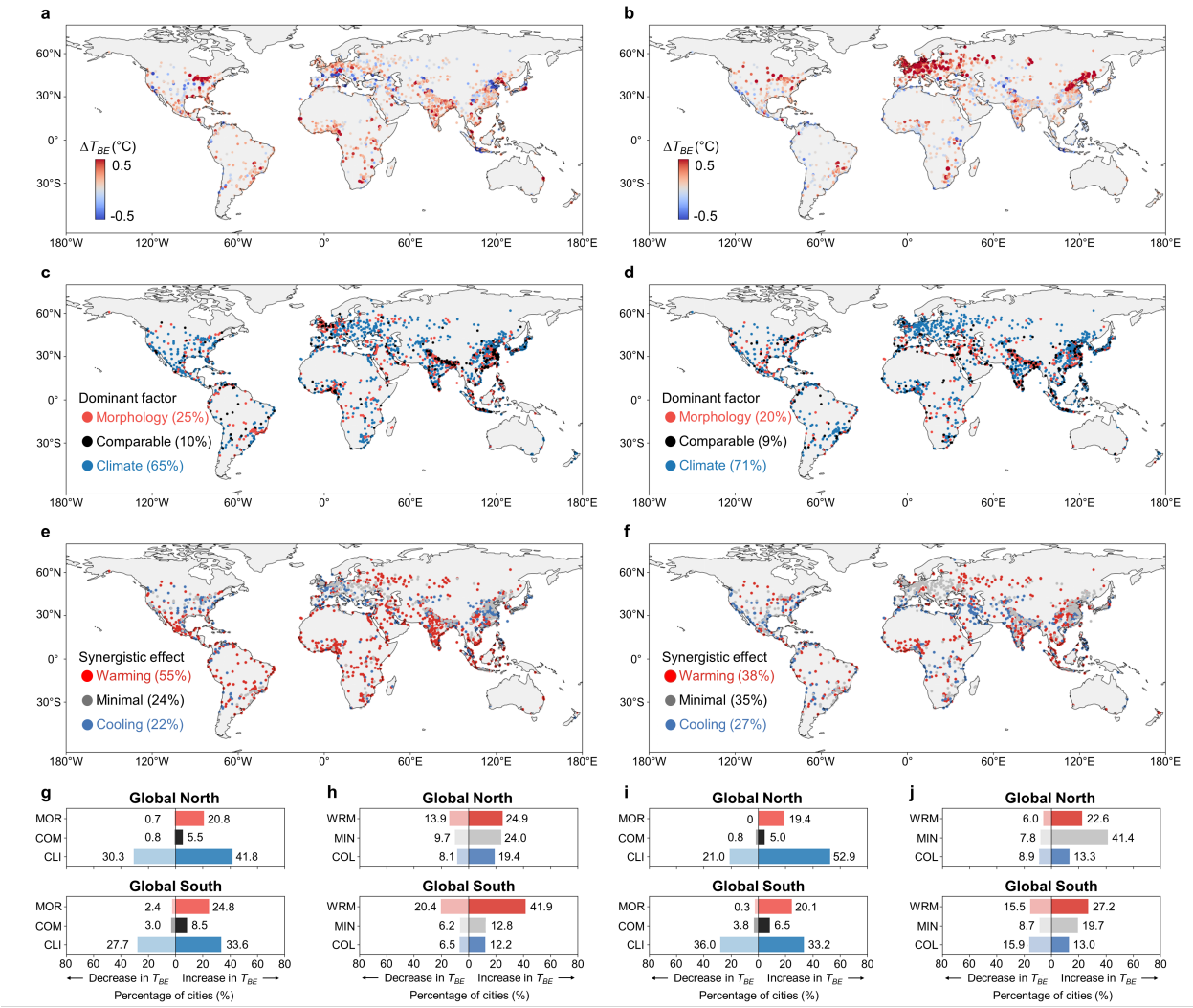

Supplementary Fig. 11 | Global distribution of projected changes in summer T_{BE} and its attribution to climate, morphology, and their interaction under SSP5 a Spatial distribution of projected differences in Summer T_{BE} (ΔT_{BE}) between present-day (2020) and future (2050) conditions for daytime. Positive values indicate an intensification of T_{BE}, whereas negative values indicate a weakening. **c** Spatial distribution of dominant driver of projected daytime T_{BE} change: Morphology (MOR), Comparable (COM), or Climate (CLI). Numbers denote the proportion of all 2,213 cities assigned to each category. Dominance was quantified using a normalized score based on the relative absolute magnitudes of the climate-only and morphology-only contributions. The climate-only contribution was calculated by applying future long-term climate conditions while holding urban morphology constant at its present state, whereas the morphology-only contribution was calculated by applying future urban

morphological conditions while holding climate constant. Cities are classified as Climate when the score is > 0.1, Morphology when it is< -0.1, and Comparable when it falls within ± 0.1 of zero. **e** Synergistic effect between climate change and urban morphological change on projected daytime T_{BE} change, calculated as the residual between projected T_{BE} under future conditions and the sum of the climate-only and morphology-only change. Numbers indicate the percentage of all 2,213 cities assigned to each synergistic class. Synergistic effects are defined using the same threshold: Warming (WRM) for values > 0.1, Cooling (COL) for values < -0.1, and minimal (MIN) interaction for values within ± 0.1. **g, h** Percentage of cities in each dominant-driver category (**g**) and synergistic-effect category (**h**) for the Global North and Global South under daytime conditions. Darker shading indicates increasing T_{BE} and lighter shading indicates decreasing T_{BE}. **b, d, f, i,** and **j** Same as **a**, **c, e, g,** and **h**, but for nighttime conditions. Basemap from Natural Earth (https://www.naturalearthdata.com).

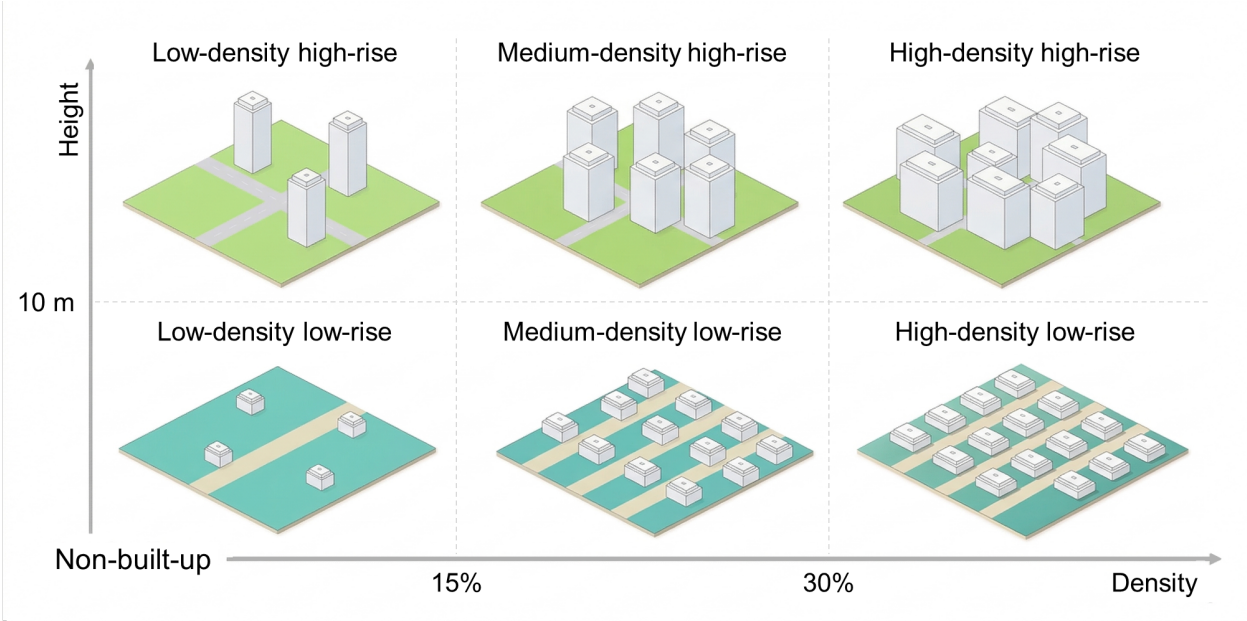

Supplementary Fig. 12 | Conceptual schematic of the six built-up types used in this study. Urban morphology was classified using three density classes based on built-up surface fraction per 1-km pixel—low (<15%), medium (15–30%), and high (≥30%)—and two height classes based on building height proxy—low-rise (<10 m) and high-rise (≥10 m), following previous studies[3–4]. Combining these dimensions yields six urban form types. Pixels with built-up surface below 2% were treated as non-built-up.

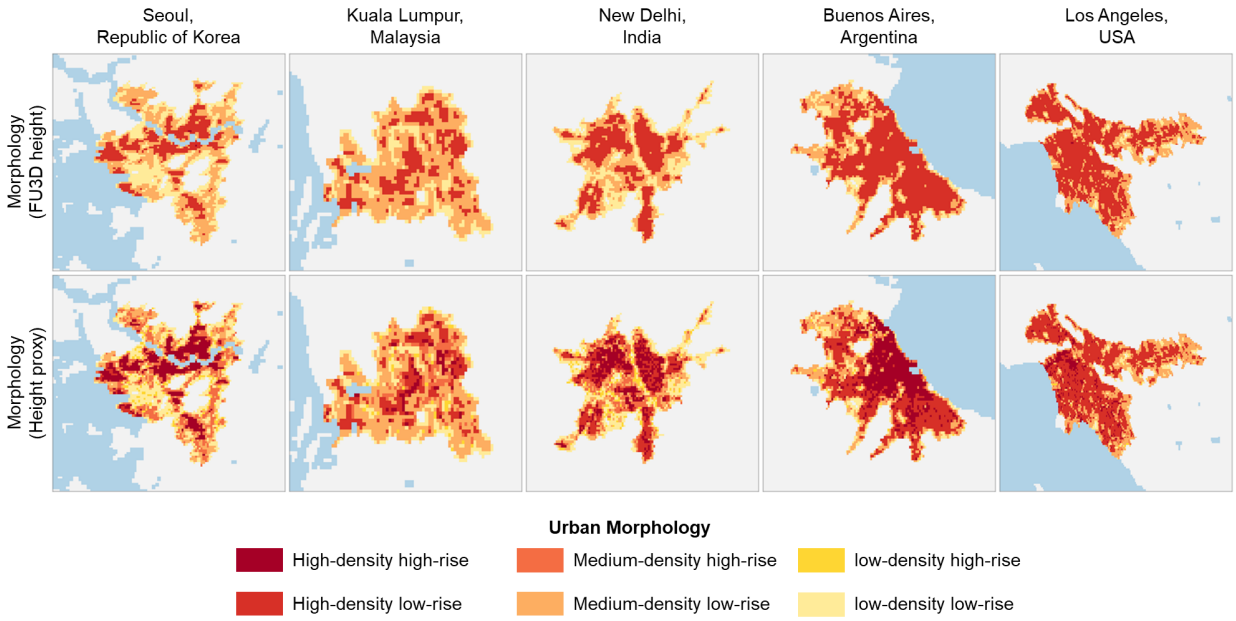

Supplementary Fig. 13 | Comparison of urban morphology maps derived from FU3D height and the volume-to-built-surface height proxy. Urban morphology maps for five representative cities (Seoul, Republic of Korea; Kuala Lumpur, Malaysia; New Delhi, India; Buenos Aires, Argentina; and Los Angeles, USA) within their urban boundaries are shown based on Global Human Settlement Urban Centre Database[1] in 2020. The top row shows morphology classes derived from the FU3D height layer[5] integrated with GHSL built-up surface fraction, whereas the bottom row shows the corresponding classes derived from a height proxy calculated as FU3D built-up volume divided by GHSL built-up surface. Colors indicate the six urban morphology classes; blue denotes water, and grey denotes land outside the GHSL urban center boundary. Basemap from Natural Earth (https://www.naturalearthdata.com).

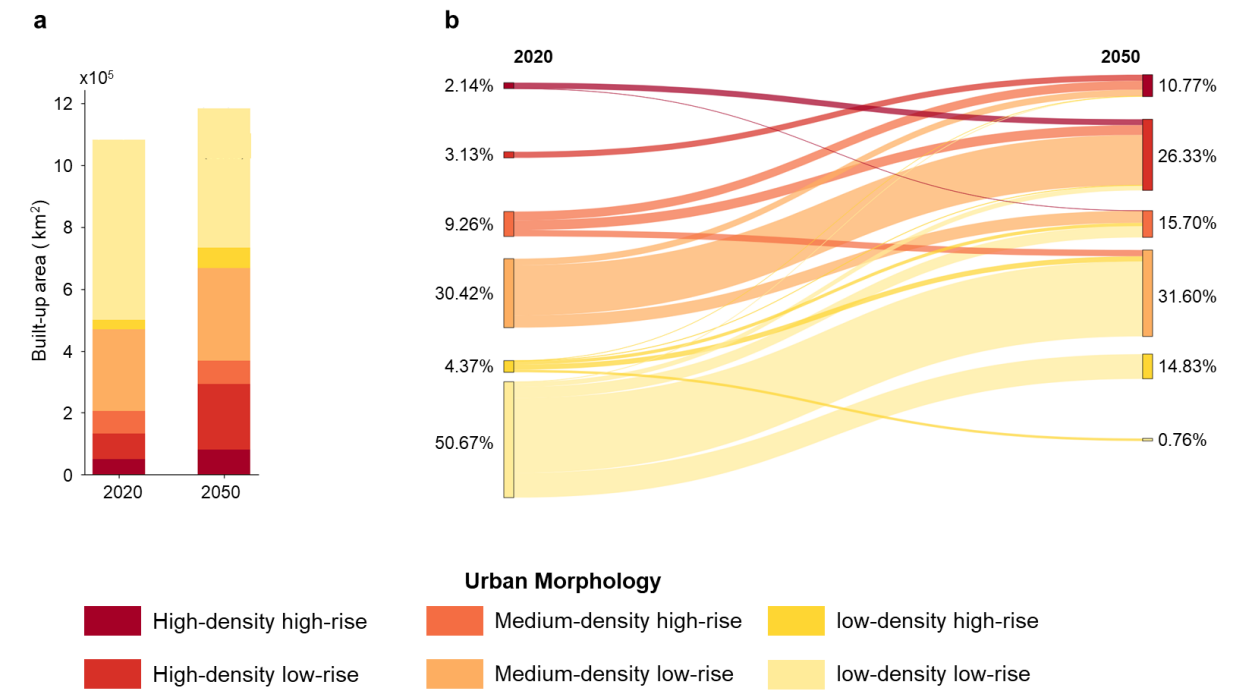

Supplementary Fig. 14 | Projected changes in urban extent and morphology from 2020 to 2050. a Total built-up area by urban morphology class in 2020 and 2050 under SSP2 scenario. **b** Transitions in urban morphology classes between 2020 and 2050. Flows indicate changes in built-up area from one urban form type to another. Colors denote the six built-up types.

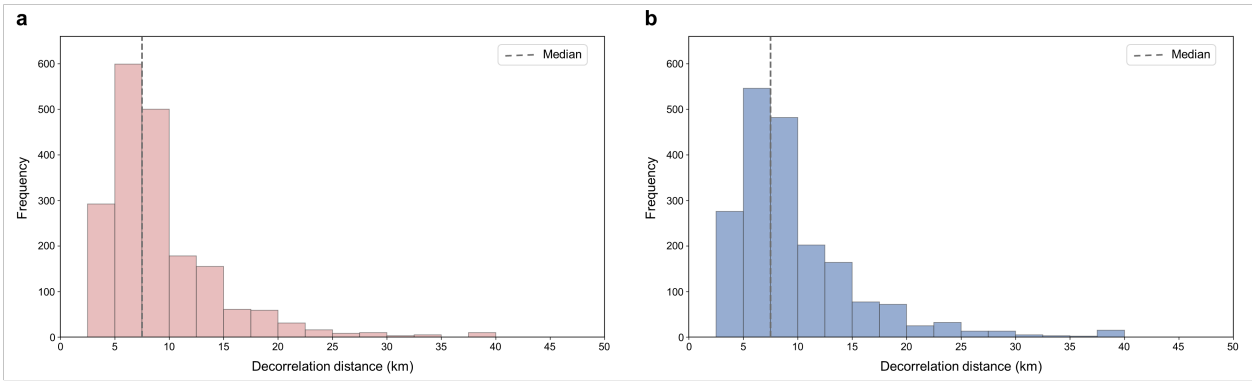

Supplementary Fig. 15 | Distribution of city-level decorrelation distance for pixel-level urban heat island intensity during daytime and nighttime. a Daytime, **b** Nighttime. For each city, the decorrelation distance was defined as the first spatial distance bin where the absolute pairwise correlation in pixel-level UHI intensity fell below 0.05. Dashed vertical lines indicate the median decorrelation distance across cities.

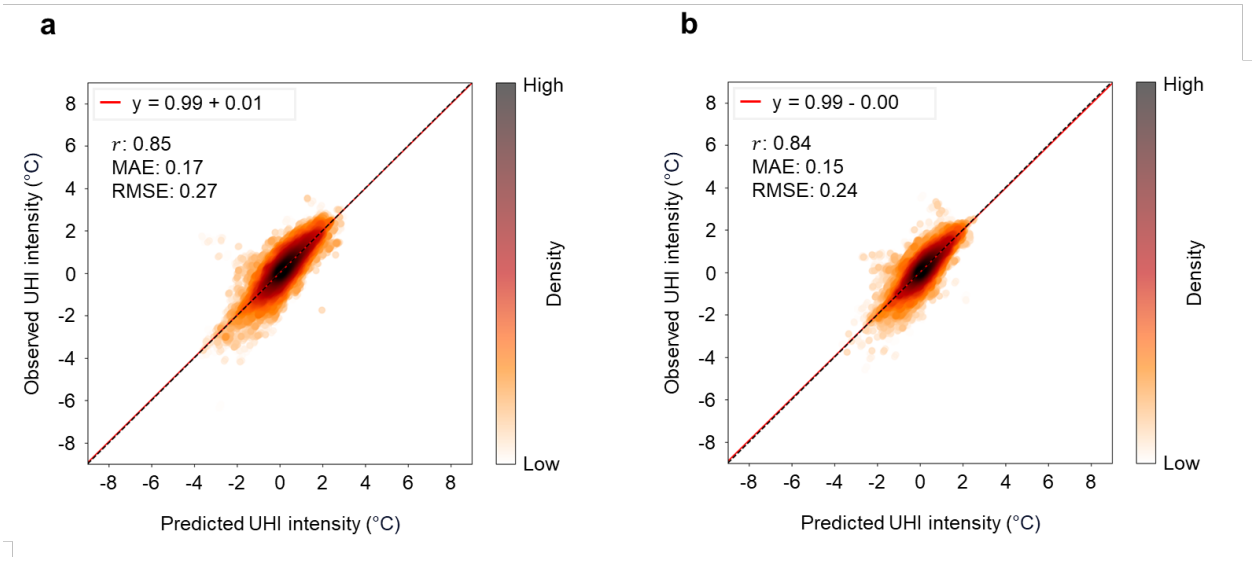

Supplementary Fig. 16 | Model performance in predicting canopy urban heat island (UHI) intensity using eXtreme Gradient Boosting (XGB). a, b, Density scatter plots comparing predicted and observed UHI intensity for daytime (**a**) and nighttime (**b**). Point density is indicated by color, with lighter shades representing lower density and darker shades representing higher density. Red lines denote linear regression fits, with equations shown in each panel. Model performance is evaluated using the Pearson correlation coefficient (r), mean absolute error (MAE), and root mean squared error (RMSE).

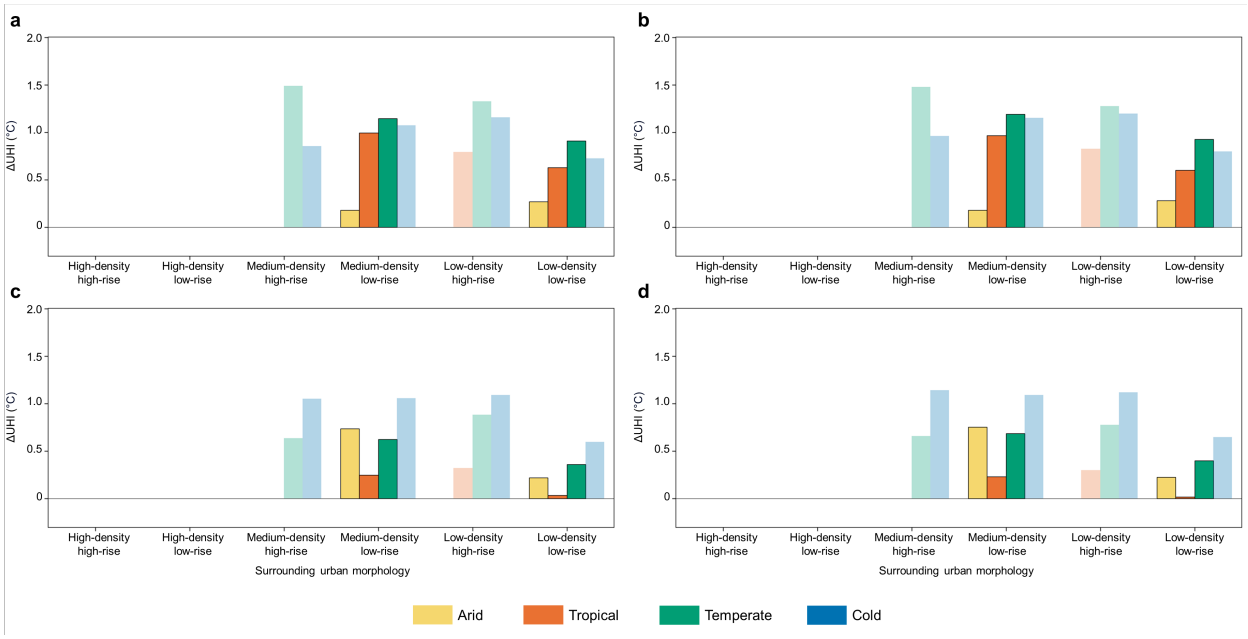

Supplementary Fig. 17 | Observed and predicted surrounding urban morphology-induced urban heat island change (ΔUHI) across climate zones. a, c Observed ΔUHI during daytime (**a**) and nighttime (**c**). **b, d** Predicted

ΔUHI during daytime (**b**) and nighttime (**d**). Bars with black outlines indicate urban structures with sufficient sample size ($n \geq 20$), while bars without outlines and reduced opacity represent those with limited data ($n < 20$). All comparisons were conducted under the same observable ΔUHI conditions across cities, ensuring a consistent and equitable basis for evaluating model predictions.

Supplementary Table 1 | Classification thresholds and number of cities in each built environment-weighted thermal effects (T_{BE}) category by climate zone. Thresholds were determined using Jenks natural breaks classification, applied separately to daytime and nighttime T_{BE} values.

Time	T_{BE}	Arid	Tropical	Temperate	Cold	Total
Day	Low	285	250	363	28	926
	Moderate	98	279	445	211	1,033
	High	20	20	138	76	254
	Total	403	549	946	315	2,213
Night	Low	136	444	490	96	1,166
	Moderate	224	92	387	192	895
	High	43	13	69	27	152
	Total	403	549	946	315	2,213

Supplementary Table 2 | Comparison of predictive performance across alternative surrounding extents. Model performance for different surrounding window sizes was evaluated using the same sample set, with the Pearson correlation coefficient (r), mean absolute error (MAE), and root mean squared error (RMSE) used as evaluation metrics.

Time	Spatial extent	r	MAE	RMSE
Day	3x3	0.883	0.163	0.254
	5x5	0.886	0.161	0.252
	7x7	0.886	0.162	0.252
Night	3x3	0.881	0.145	0.221
	5x5	0.887	0.141	0.215
	7x7	0.890	0.139	0.213

Supplementary References

1. Melchiorri, M. et al. *Stats in the City–the GHSL Urban Centre Database 2025* (European Commission, 2024).
2. Beck, H. E. et al. High-resolution (1 km) Köppen-Geiger maps for 1901–2099 based on constrained CMIP6 projections. *Sci. Data* **10**, 724 (2023).
3. Chen, T. H. K. et al. Mapping horizontal and vertical urban densification in Denmark with Landsat time-series from 1985 to 2018: a semantic segmentation solution. *Remote Sens. Environ.* **251**, 112096 (2020).
4. Chen, T. H. K. et al. Higher depression risks in medium-than in high-density urban form across Denmark. *Sci. Adv.* **9**, eadf3760 (2023).
5. Zhao, Q., Meng, Q., Gao, L. & Zhu, M. FU3D: the first global projections of future urban three-dimensional (3D) expansion for the 21st century under shared socioeconomic pathways. *Sci. Data* **12**, 1555 (2025).